Appendix

เอกสารแนบหมายเลข 1

AGU PUBLICATIONS

JGR

Journal of Geophysical Research: Space Physics

TECHNIQUE

10.1002/2013JA019641

Key Points:
- Taylor microscale is important in turbulence
- Measurement is hindered by finite time resolution data
- Technique given here improves estimates

Correspondence to:
W. H. Matthaeus,
whm@udel.edu

Citation:
Chuychai, P., J. M. Weygand, W. H. Matthaeus, S. Dasso, C. W. Smith, and M. G. Kivelson (2014), Technique for measuring and correcting the Taylor microscale, *J. Geophys. Res. Space Physics*, *119*, doi:10.1002/2013JA019641.

Received 21 NOV 2013
Accepted 4 MAY 2014
Accepted article online 8 MAY 2014

Technique for measuring and correcting the Taylor microscale

P. Chuychai[1,2], J. M. Weygand[3], W. H. Matthaeus[4], S. Dasso[5], C. W. Smith[6], and M. G. Kivelson[3]

[1]School of Science, Mae Fah Luang University, Chiang Rai, Thailand, [2]Thailand Center of Excellence in Physics, CHE, Ministry of Education, Bangkok, Thailand, [3]Institute for Geophysics and Planetary Physics, University of California, Los Angeles,California, USA, [4]Bartol Research Institute, Department of Physics and Astronomy, University of Delaware, Newark, Delaware, USA, [5]Instituto de Astronomia y Fisica del Espacio (CONICET-UBA) and Departamento de Fisica (FCEN-UBA), Buenos Aires, Argentina, [6]Space Science Center, University of New Hampshire, Durham, New Hampshire, USA

Abstract We discuss and develop methods to estimate and refine measurements of the Taylor microscale from discrete data sets. To study how well a method works, we construct a time series of discrete data with a known power spectrum and Taylor scale, but with various truncations of the resolution that eliminate higher frequencies in a controlled fashion. We compute the second-order structure function and correlation function, assuming that the unresolved dissipation range spectrum has various values of spectral index. A series of Taylor scale estimates are obtained from parabolic fits to subsets of the correlation function data, and these are extrapolated to the limit of zero separation. The error in this procedure, for finite time resolution sampling, depends on the spectral index in the dissipation range. When the spectral form is known, we can compute a correction factor that improves the estimate of the Taylor microscale value determined from the extrapolation method and band-limited data. Application of this technique to spacecraft observations of solar wind fluctuations is illustrated.

1. Introduction

The motivation of this study comes from recent efforts to measure the Taylor microscale in solar wind turbulence calculated using multispacecraft techniques [*Matthaeus et al.*, 2005; *Weygand et al.*, 2007, 2009, 2010, 2011; *Gurgiolo et al.*, 2013]. The Taylor scale is related to the second derivatives of the data [*Batchelor*, 1970] (also see below); therefore, it is inherently sensitive to the high-frequency spectral content of the signal. Of course, for idealized time-continuous infinite precision data, the Taylor scale may be computed. Likewise, when very high cadence measurements are available [e.g., *Alexandrova et al.*, 2009; *Sahraoui et al.*, 2009], and the spectrum is steep enough (see below), it may be possible to unambiguously determine the Taylor scale. However, for available data sets with finite time cadence, the values of the Taylor scale obtained by a straightforward evaluation may be sensitive to the data resolution, as the correct value may depend on the physical signal above the sampling Nyquist frequency.

The objective of this study is to understand the accuracy of the Taylor scale estimates using finite resolution data sets, in which the high-frequency spectra may or may not be well known. We develop a method to improve these estimates based on the spectrum of the unresolved data, which can be used when estimates of the high-frequency spectrum of the signal are available in some way, whether it be observations, theory, or an informed guess. Although the main purpose here is to discuss measurement issues, the physical significance of the Taylor scale will be reviewed briefly in section 2.

In a system such as the solar wind, the Taylor microscale can be estimated from single spacecraft analyses. Within the context of the *Taylor* [1938] frozen-in flow approximation, time t separation is converted to spatial x separation using the relation $x = V_{sw} \times t$. In the latter case, instead of working in the spatial domain, the curvature of the two time correlation near the origin can be estimated. Frozen-in flow is a standard approximation in solar wind observational analysis and in wind tunnels. *Dasso et al.* [2008] demonstrates the validity of this approximation in the solar wind by comparing values determined from single spacecraft and multispacecraft analysis. With this background in mind, one can define the Taylor microscale (λ_T) by

$$\frac{1}{\lambda_T} = \sqrt{\frac{\left\langle \left(\frac{\partial F}{\partial x}\right)^2 \right\rangle}{\langle F^2 \rangle}} \rightarrow \frac{1}{V_{sw}\tau_{TS}} = \frac{1}{V_{sw}} \sqrt{\frac{\left\langle \left(\frac{\partial F}{\partial t}\right)^2 \right\rangle}{\langle F^2 \rangle}}, \tag{1}$$

where F is the function of interest such as the velocity or magnetic field fluctuations. For generality and simplicity, here we will discuss methods for arriving at improved estimates of the Taylor scale under the assumption that the problem of interest is in the time domain or that frozen-in flow is valid. Therefore, the discussion will center on the procedure to extract τ_{TS} from a time series $F(t)$. We will employ a model spectrum in which the inertial range terminates by steepening at a "dissipation scale" (Kolmogorov scale) or its equivalent in the time domain τ_d, which is the equivalent sweeping time of the dissipation length scale past the detector. Thus, in the present paper the term dissipation scale implies only the scale at which the power law cascade range terminates, generally leading to a steeper spectrum. This familiar terminology is used in a purely kinematic sense, without regard for whether this steepening is due to dissipation, dispersion, or some other effect.

Focusing on the time domain, the Taylor microscale can be also viewed as the radius of curvature at the origin of the autocorrelation function

$$R(\tau) = \langle F(t)F(t+\tau)\rangle. \tag{2}$$

From a small τ expansion, and using $R(\tau) = R(-\tau)$, a requirement of time stationarity, the autocorrelation function near the origin, can be determined by

$$R(\tau) \approx 1 - \frac{\tau^2}{2\tau_{TS}^2} + \ldots. \tag{3}$$

Therefore, one way to obtain the Taylor microscale from measurements is to fit $R(\tau)$ at the origin. However, sometimes the observation data do not have sufficient time resolution near the origin to perform an adequate parabolic fit. This is due to the fact that for many reasonable spectra, the quadratic behavior suggested in equation (3) is not apparent until the correlation function is sampled at scales $\tau < \tau_d$. We will study the expected effects on Taylor scale determination using a designed function $F(t)$ that is intentionally undersampled but which is extracted from a signal that has better time resolution and a known spectral index in the dissipation range. This is a useful approach to develop a procedure that reliably determines the Taylor microscale. To develop this technique we construct the time data series based on a specified spectrum. With varying resolution synthetic data, we obtain empirical values of the Taylor microscale and compare with the known "exact" values. We find that it is possible to define a multiplicative correction factor that allows us in some circumstances to adjust and improve the measured Taylor scale based on assumptions about the spectrum of the unresolved high-cadence data.

Before turning to the main content of the paper, we digress briefly concerning the physical significance of the Taylor scale, both in hydrodynamics [*Batchelor*, 1970] and in the case of collisionless plasma such as the solar wind. In isotropic hydrodynamic turbulence, the Taylor scale may be defined as the radius of curvature at the origin of the two-point velocity ($\mathbf{v}$) correlation $R(r) = \langle \mathbf{v}(0)\cdot\mathbf{v}(\mathbf{r})\rangle$; that is, $\lambda_T^2 = R(0)/R''(0)$ or equally well as the length associated with the mean square curl of the velocity (the vorticity), $\lambda_T^2 = \frac{\langle|\mathbf{v}|^2\rangle}{\langle|\nabla\times\mathbf{v}|^2\rangle}$. For viscous ($\nu$) dissipation in an incompressible medium, the Taylor scale is also related to dissipation, in that (for suitable boundary conditions), $\frac{d\langle|\mathbf{v}|^2\rangle}{dt} = -\nu\lambda_T^{-2}\langle|\mathbf{v}|^2\rangle$. In this sense the Taylor scale is the "equivalent dissipation scale," in that, any instant of time, the dissipation rate is the same as if all the energy were at the Taylor scale. In older turbulence texts [*Hinze*, 1975] the Taylor scale is sometimes designated simply as "the dissipation scale." However, in more current terminology the latter is usually reserved for the Kolmogorov scale η which signifies the scale (or wave number $1/\eta$) at which the power law inertial range terminates and beyond which lies the dissipation range. For high Reynolds number R and correlation scale L, in hydrodynamics, the Taylor scale is $\lambda_T = L/\sqrt{R}$, while $\eta = L/R^{3/4}$. Therefore, $\lambda_T/\eta = R^{1/4}$, and the two become well separated at very large R. For plasmas the dynamical status of both the Taylor scale and the Kolmogorov scale becomes ambiguous [see, e.g., *Matthaeus et al.*, 2008]. The mechanism of dissipation is not well understood for collisionless plasma and may vary in different parameter regimes. Thus, λ_T cannot be interpreted as connected with the length scale or rate of energy dissipation. Likewise, the termination of the inertial range may not be associated with dissipation, as the onset of kinetic dispersive waves may also be influential. Nevertheless, it is convenient to maintain the kinematic definitions of Taylor scale and "dissipation scale," related respectively to the second derivative of the correlation function at the origin and the termination of the inertial range. In the remainder of the paper we adopt the kinematic meaning of λ_T and the dissipation scale, as well as their time domain counterparts, to be defined below.

2. Generating Discrete Data With a Known Taylor Scale

To develop our method, we use synthetic data generated using a known spectrum and then employ a typical methodology to evaluate the Taylor microscale. The spectrum is constructed with inertial and dissipation ranges that have been independently controlled and have generally different power law indices. To be specific, we let the inertial range have a spectral index of $-5/3$, while the dissipation range has an adjustable spectral index q. The particular functional form of the spectrum is

$$P(f) = \begin{cases} \frac{C}{[1+(f\tau_0)^2]^{5/6}}, & \text{where } f_{\min} < f \le f_d \\ \frac{C}{[1+(f_d\tau_0)^2]^{5/6}} \left(\frac{f_d}{f}\right)^q, & \text{where } f_d < f \le f_e \\ 0, & \text{where } f_e < f \le f_{\max}, \end{cases} \tag{4}$$

where $q < 0$. The reasons for these choices are as follows: First, the flat spectral region at very low frequencies $f\tau_0 << 1$ is designed to make the signal time stationary. This is unrealistic for the solar wind, which has very low frequency components due to, e.g., solar rotation and solar cycle [see, e.g., *Matthaeus and Goldstein*, 1982]. However, we are not concerned with very low frequency effects here. Second, the inertial range with Kolmogorov spectral index of $\sim 5/3$ is found for higher frequencies, at $f\tau_0 > 1$. Third, there is a discontinuous jump at the top of the inertial range at frequency f_d, the slope steepening from $-5/3$ to $-|q|$, in qualitative accord with observations [*Leamon et al.*, 1998; *Hamilton et al.*, 2008; *Alexandrova et al.*, 2009; *Sahraoui et al.*, 2009]. Finally, at high frequencies $f > f_e$ we set the spectrum to zero, for numerical rather than physical reasons, to provide a very smooth trigonometric interpolation of the signal at the grid scale.

Adopting illustrative values that are representative of the solar wind at 1 AU, we assume that the spectrum starts from $f_{\min} = 1.22 \times 10^{-5}$ Hz and is flat until $f_0 = 1/\tau_0 = 3.906 \times 10^{-4}$ Hz, a "bendover" frequency often associated with the correlation scale or coherence time. Thereafter, the spectrum has an inertial range with a 5/3 power law index, until a second breakpoint is encountered at $f_d = 1/\tau_d = 0.4$ Hz. For historical reasons, this breakpoint, which terminates the power law MHD-scale inertial range, is often referred to as the dissipation scale [*Leamon et al.*, 1998], although it is also possible that it characterizes dispersion in addition to dissipation [*Gary and Borovsky*, 2004]. In the hydrodynamic case the eddy turnover time and viscous dissipation time scales become equal at the dissipation scale. However, for the solar wind or other low-collisionality astrophysical plasmas, it is unclear whether the fluctuations become critically damped at the breakpoint/dissipation scale. For example, the inertial range is typically found to terminate near the proton gyroscales, and while some dissipation may occur at such scales, further kinetic plasma dynamics may transfer energy to higher frequencies until much smaller electron scales are encountered [*Alexandrova et al.*, 2009; *Sahraoui et al.*, 2009]. It has been argued that a substantial fraction of actual dissipation may occur due to electrons. In any case the scale f_d corresponds to the onset of kinetic processes and the end of the Kolmogorov-like inertial range. It is, however, the kinematic properties of the spectrum that come into play in the current study, rather than the dynamical origin of the spectral forms.

In our model beyond the breakpoint f_d, we extend the dissipation range with power law index q until $f_e = 16.0$ Hz. This may be considered in the solar wind application to be associated with the electron dissipation scale. The spectrum cuts off completely at $f_{\max} = 25.6$ Hz. To decide upon these numerical values, here we assume that the dissipation scale and electron dissipation scale correspond to the proton and electron inertial scales, respectively. Thus, we set $f_e/f_d = 40$ to be consistent with the ratio of electron and proton inertial scales in MHD, which is about $\sqrt{m_p/m_e} = 42.9$ [see, e.g., *Sahraoui et al.*, 2009].

Once we have specified the spectrum, we generate realizations of the signal in the frequency domain, $F(f)$, as

$$F(f) = \sqrt{P(f)} \exp\,[i\phi] \tag{5}$$

where ϕ is a random phase. Then a fast Fourier transform is used to convert the function $F(f)$ into the real-time domain. In the simulations reported here, we employ this approach to obtain 2^{22} data points for the time series.

Table 1. Showing Index q Which We Vary for Each Case and Their Taylor Scales When We Fix the Dissipation Scale (τ_d) = 2.5 s

case	τ_{TS}^{expect} [s]	τ_{TS}^{expect} [τ_d]
$q = -\infty$	6.569	2.63
$q = -5$	5.097	2.04
$q = -4$	4.368	1.75
$q = -3$	2.869	1.15
$q = -7/3$	1.607	0.64
$q = -2$	1.095	0.44
$q = -1$	0.095	0.028

We next compute the Taylor microscale from the data set we generated by employing the definition equation (1). In Table 1, we give the Taylor microscale values for a range of dissipation scale indices q corresponding to the generic power spectrum shown in Figure 1. (Note that the spectra are given here as Fourier amplitudes squared, which can easily be converted to power spectral density.) We will treat these expected values of the Taylor microscale as the true or exact Taylor microscale values for the synthetic time series data. To examine and test our extrapolation method, we use only one eighth of the original data. The purpose of defining this subset is that any consistent method will provide good (and even convergent) values of τ_{TS} when the time resolution Δt of the estimates is very fine, i.e., the spectral cutoff is resolved and $\Delta t f_{max} < 1/2$. However, our motivation is to obtain reasonably accurate values of τ_{TS} when the effective resolution of the data sampling is adjusted so that we are not in this asymptotic regime—a circumstance that is more likely to be realized in practice when analyzing spacecraft data.

With the subset of our discrete time series, we compute the second-order structure function. This can be used to obtain an estimate of the correlation function. We then determine the radius of curvature from correlation function and an estimate of the Taylor microscale. In the following section, we will demonstrate an extrapolation technique [*Weygand et al.*, 2007, 2009, 2010, 2011] to estimate Taylor microscale from a series of parabolic fits of the correlation function near the origin. The details of the method we use are given in the following subsections.

2.1. Correlation Function and Structure Function

In estimating the correlation function from many samples of data, it is useful to employ the normalized correlation function

$$\hat{R} = \frac{R}{\langle [F(t)]^2 \rangle}. \tag{6}$$

This reduces errors associated with variability of the variance, i.e., the fluctuation energy. Almost the same information is contained in the second-order structure function S_2, given by

$$S_2(\tau) = \langle [F(t+\tau) - F(t)]^2 \rangle. \tag{7}$$

In fact,

$$\hat{R}(\tau) = 1 - \frac{S_2(\tau)}{2\langle F(t)^2 \rangle}. \tag{8}$$

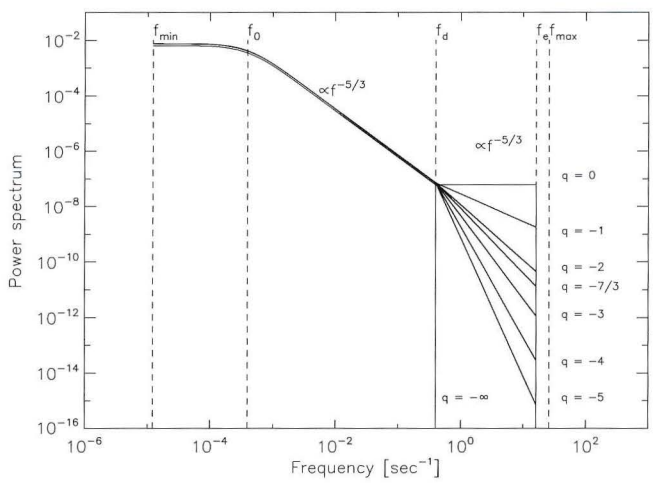

Figure 1. The power spectrum for a number of values of q in the dissipation range.

Figure 2 shows the structure functions for various dissipation range indices q that we generated as described in section 2. Note that values of dissipation range spectral index in the range $-5/3 < q < -1$ are pathological in that the implied "dissipation range" has either the same or shallower spectral power law than that found in the inertial range. These values are included only for illustration. As q is varied, several regimes are seen:

1. For $\tau \gg \tau_d$, which is associated with the inertial range ($f^{-5/3}$) in Fourier space, one expects to find $S_2 \propto \tau^{2/3}$.
2. For $\tau \ll \tau_d$ and with $q = -5$ and -4, one finds (see Figure 2) that $S_2 \propto \tau^2$.

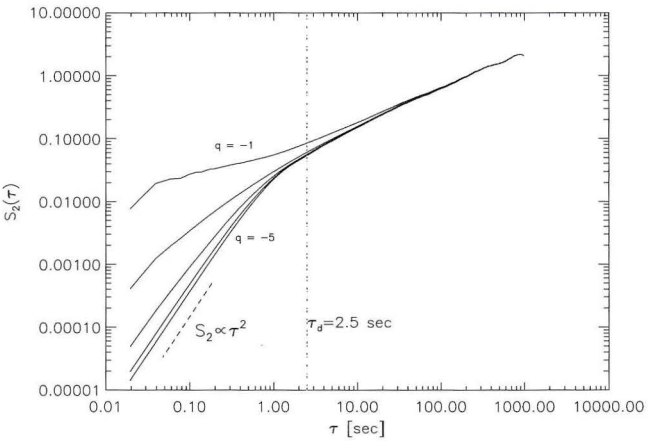

Figure 2. The structure function computed from the time series data for a number of values of q. The bottom curve is associated with a q value of −5, and the higher curves are determined with $q = -4, -3, -2$, and −1, respectively.

This is the regime, in accordance with equation (8), in which parabolic curvature of the correlation function is seen near $\tau = 0$.

3. For $\tau \ll \tau_d$, but q values of −3 or shallower, the required parabolic behavior is not seen near τ_d, but rather this asymptotic behavior is deferred until $\tau < 1/f_e$. This is due to the fact that the spectrum for this range of q is not steep enough to cause convergence of the Taylor scale estimate. This convergence is now delayed until scales are sampled that are finer than the electron dissipation scale.

This change in behavior of Taylor scale estimates as the dissipation range spectral index is varied and is actually very relevant to solar wind observations. For scales smaller than ion inertial length, the solar wind spectral slope is found to be quite variable. For example, *Smith et al.* [2006b] estimate that dissipation range magnetic spectral indices are broadly distributed with average values $|q| = 2.61 \pm 0.96$ for intervals lacking magnetic clouds, and $|q| = 2.01 \pm 0.84$ for cloud intervals.

A lesson can be learned from the above simple exercise: the asymptotic form of the correlation function embodied in equations (3) and (8) is not obtained until the sampled spectrum is k^{-4} or steeper. Between spectral indices −4 and −3, the transition to the asymptotic parabolic form migrates toward finer scales, until at k^{-3}, the transition is delayed until separations within the assumed inner cutoff scale are sampled.

From equation (8), we can compute the correlation function from the structure function. Figure 3 displays the correlation function for various q. From these plots, we can see that the correlation function has a parabolic shape at the origin. At this fixed resolution, the characteristic parabolic shape becomes better defined as the values of $|q|$ are increased.

Suppose now we select a known q and we compute the radius of curvature of the correlation function from data over a range of small separations near the origin $0 < \tau \leq \tau_{\text{fit}}$. While this value is intended to be small, to attempt to capture the parabolic regime (if present), the specific value τ_{fit} has no physical significance—it is just a maximum lag to be used in a fitting procedure. This choice of a range of data provides an estimate of τ_{TS}; let us call it $\tau_{\text{TS}}^{\text{est}}(\tau_{\text{fit}})$. At this point we have obtained an approximate fit, or representation, of the data in this range of τ, given by

$$\hat{R}(\tau) = 1 - \frac{\tau^2}{2\left[\tau_{\text{TS}}^{\text{est}}(\tau_{\text{fit}})\right]^2}. \quad (9)$$

This fit is inexact even if the measurements are perfect, because we expect that the Taylor scale is $\tau_{\text{TS}} = \lim_{\tau_{\text{fit}} \to 0} \tau_{\text{TS}}^{\text{est}}(\tau_{\text{fit}})$. It is not practical to compute this limit because the data has finite time resolution Δt and because there may be limited data available at the shortest time lags. In another section below we will systematically examine the influence of Δt, the data sampling time.

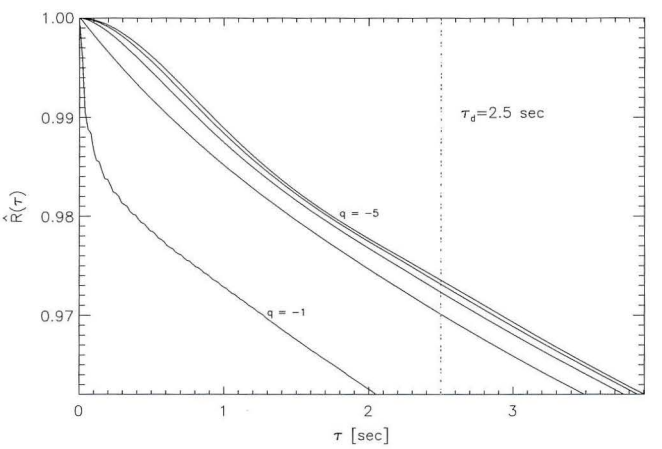

Figure 3. The correlation function near the origin. The top curve is determined from $q = -5$ and the next curves are calculated using $q = -4, -3, -2$, and −1, respectively.

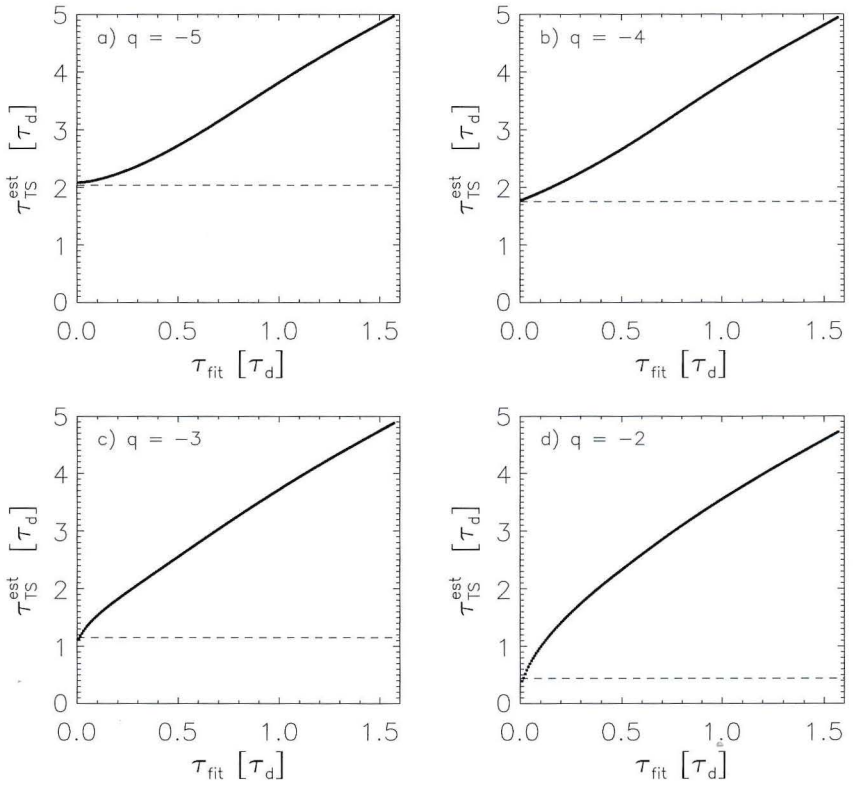

Figure 4. Taylor microscale from parabolic fit of the correlation function near the origin for each τ_{fit} for a number values of q. Axes are in units of τ_d. Dashed line indicates the exact Taylor microscale.

What can be done, however, is to compute $\tau_{TS}^{est}(\tau_{fit})$ for a range of τ_{fit} and to examine the trend of the corresponding values of τ_{TS}^{est} as the maximum lag used in the fit becomes smaller. Figure 4 illustrates sequences of such fits $\tau_{TS}^{est}(\tau_{fit})$ versus τ_{fit}. Each of these curves approaches the exact value of Taylor scale in the limit of zero τ_{fit}, as expected. This is for an idealized model times series that can be evaluated at any time separation we wish. Consequently, when a range of τ_{TS}^{est} is available, but only for a set of values of τ_{fit} that excludes the origin, one can try to recover a more precise value of τ_{TS} by an extrapolation technique that provides a refined estimate of the radius of curvature at the origin.

2.2. Extrapolation Method

To obtain a stable value for the Taylor microscale at $\tau = 0$, we apply a method based on the Richardson extrapolation technique [see *Dahlquist and Bjorck*, 2003] in analogy with similar procedures employed in numerical analysis. In the first step we compute a series of parabolic fits to data near the origin, and for varying values of τ_{fit}, up to a largest values of τ_{fit}, say, τ_{max}. Using the available estimated values of Taylor microscale $\tau_{TS}^{est}(\tau_{max})$ for this range of τ_{max}, we can compute a straight line extrapolation of the Taylor scale back to the origin ($\tau_{fit} = 0$). This extrapolation gives a single estimate of a refined value of the Taylor microscale.

Still, it remains unclear which value of τ_{max} we should use. On the one hand, a larger τ_{max} permits the use of more data in the fit process, but a smaller τ_{max} moves us closer to the asymptotic range in which the formula equation (9) for approximating the radius of curvature at the origin becomes more exact. Therefore, we will look for a stable range of values, as follows.

Figure 5 illustrates the variation of the extrapolated values of Taylor microscale as the value of τ_{max} is varied. In the next step of the method we examine whether for some range of τ_{max} we find a stable value of estimated τ_{TS}^{est}. When working with real data with time cadence Δt, this process is constrained by the temporal resolution, i.e., $\tau_{fit} > \Delta t$. The distribution of number of available estimates at each lag τ can also become an issue. In addition, the quality of the refinement of the Taylor microscale value will depend on the steepness of the spectrum (i.e., q) at the high frequencies.

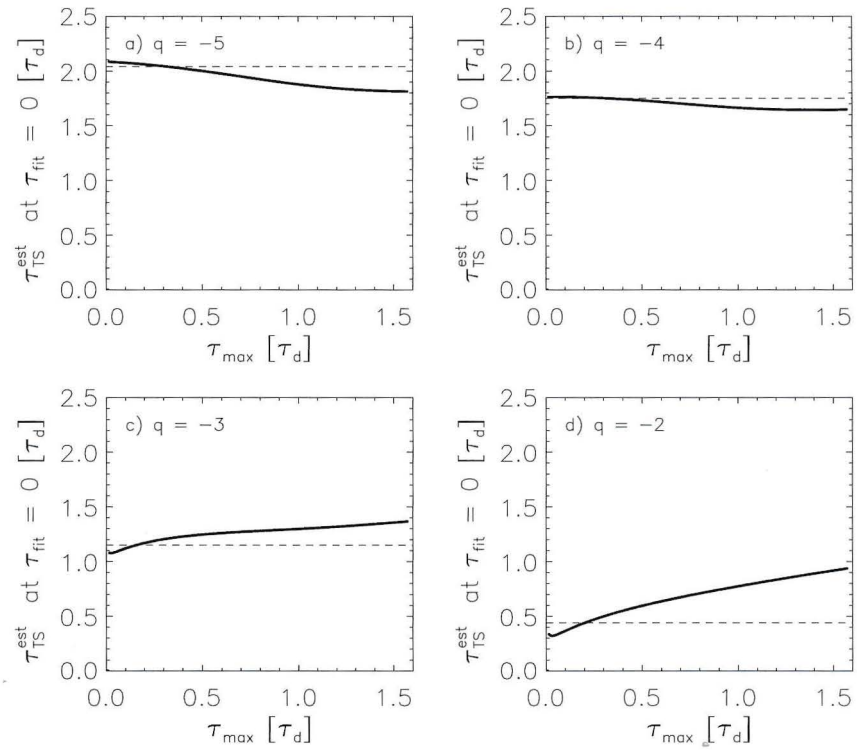

Figure 5. Values of τ_{TS} determined by linear extrapolation from the data in Figure 4 at the origin (i.e., the intercept). Plotted are the extrapolated Taylor microscale values determined from a range of τ_{max}.

In the next section we will discuss more details regarding the effects of data resolution and q. For now, (see Figure 5) we can make some general statements regarding quality of estimation when a range of estimates is available for time lags near the dissipation (spectral steepening) scale. For large values of $|q|$, where the correlation function has a large radius of curvature at the origin (compared to τ_d), we find a stable value of the Taylor microscale as τ_{max} approaches zero. In contrast, for small values of $|q|$, we do not obtain a stable value of τ_{TS} after the extrapolation.

One can also see by examining Figure 5 how lower time resolution data can have an adverse effect. Larger Δt means that the data close to the origin become unavailable for the extrapolation near $\tau_{fit} = 0$. The best we might be able to do in such cases is to choose a stable value in the range of τ_{max} to τ_d. By trying this out with the graphs, we see that this approach yields an underestimate of the Taylor microscale value when $|q|$ is approximately greater than 4 and an overestimate when $|q|$ is approximately less than 4. Our results suggest that a good estimate of τ_{TS} is obtained by a linear extrapolation to zero lag using the slope of the curves $\tau^{est}(\tau_{fit})$ evaluated near $\tau_{max} = \tau_d$ (see Figure 4). In the next subsection we will discuss how we can further improve this estimate with a correction ratio that takes into account known information about the spectra at higher frequencies.

2.3. Correction Ratio

The resolution of the observational data is limited by the instrumentation, the spacecraft data downlink, and spacecraft data storage. The lower resolution of the data is the less accurate the Taylor microscale value will be, since the measurements become less sensitive to the radius of curvature of the correlation function at the origin. In this section, we examine the effect of the temporal resolution of the data by artificially reducing the resolution of the synthetic time series and again estimating the Taylor microscale with the same method. The new values for each resolution of the data can be compared with the expected Taylor microscale value to assess the impact of the temporal resolution. In particular, the ratio $\tau_{TS}^{expect}/\tau_{TS}^{est}$ is of interest. We call this ratio a "correction factor" as it can be employed to estimate the actual Taylor scale given the value computed from finite time resolution data. However, this correction must assume knowledge of the spectrum at unresolved frequencies. Here that amounts to knowledge of the value of q.

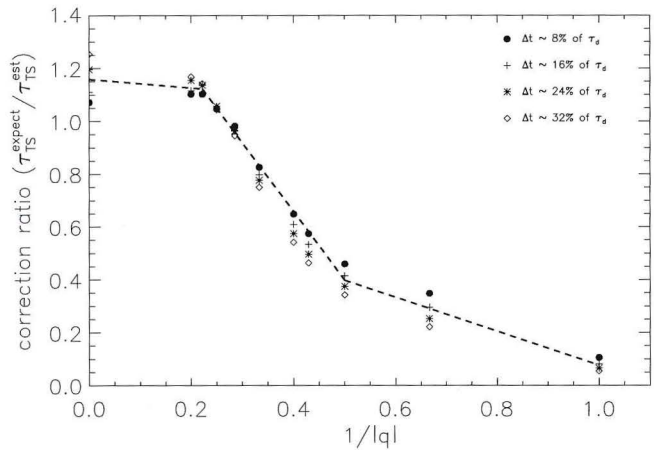

Figure 6. Correction ratio versus $1/q$ for number of different Δt values.

Figure 6 demonstrates the variation of the correction factor when we vary the temporal resolution Δt and the spectral index $|q|$. We can see that the correction ratio strongly depends on $|q|$. There are three regimes of behavior apparent in the figure, which we approximate as a piecewise linear function. The model suggests a correction for the Taylor scale estimates obtained from finite time resolution data. Accordingly, the empirical correction factor $r(|q|)$ can be written as

$$r(|q|) = \begin{cases} -0.64\left(\frac{1}{|q|}\right) + 0.72, \text{ when } |q| < 2 \\ -2.61\left(\frac{1}{|q|}\right) + 1.70, \text{ when } 2 \le |q| < 4.5 \\ -0.16\left(\frac{1}{|q|}\right) + 1.16, \text{ when } |q| \ge 4.5. \end{cases} \quad (10)$$

With this model for a given data set and a known value of q, it is possible to compute a corrected value of the Taylor microscale using

$$\tau_{TS} \approx r(|q|)\tau_{TS}^{extra} \quad (11)$$

where τ_{TS}^{extra} is an estimate obtained by the extrapolation method described in section 2.2 above. This procedure presupposes that sufficient data are available to approximately determine the asymptotic tendencies of the correlations. From a practical perspective this appears to require that information about the functions near the dissipation scale τ_d be included in the analysis. Based on the present numerical experiments, we recommend therefore that the resolution of the data be at least as good as $\Delta t < 0.4\tau_d$.

3. Applying the Technique to Spacecraft Data

From an analysis of the magnetic field data from the ACE spacecraft [*Smith et al.*, 2006a], the Taylor microscales in the left column of Figure 7 are determined by employing the extrapolation method described above but without applying the correction ratio. We use the same data set of ACE observations as was employed by *Smith et al.* [2006a, 2006b] and *Hamilton et al.* [2008]. The time resolution of the ACE data used here is $\delta t = 0.333$ s or three vectors per second. The analysis of the ACE proceeds in the following way: The second-order structure function matrix is computed for each interval in the set of intervals studied. The Taylor scale is then estimated using a series of maximum lag approximations from a maximum lag of four data points to a maximum lag of 25. A line is fit to these estimated values of the Taylor scale as a function of maximum lag, and the lag = 0 intercept is computed. This gives the final estimated values shown in the figure. The dissipation scale is computed from the power spectrum as the intercept between two fit lines, one describing the ion inertial range frequencies and the other describing the ion dissipation range frequencies. The dissipation range spectral index q is determined from the short wavelength fit.

The black color shows the data from regions characterized as open magnetic field line regions, and the red color shows the data from magnetic clouds (closed field regions). The Taylor scales have already been converted to spatial scales by using the frozen-in approximation.

The values obtained for dissipation range spectral index lie between −5 and −1, and the ratio of Taylor scale (λ_T) to the dissipation scale (λ_d) ranges between 0.1 and 10. The individual plots show that the red and black

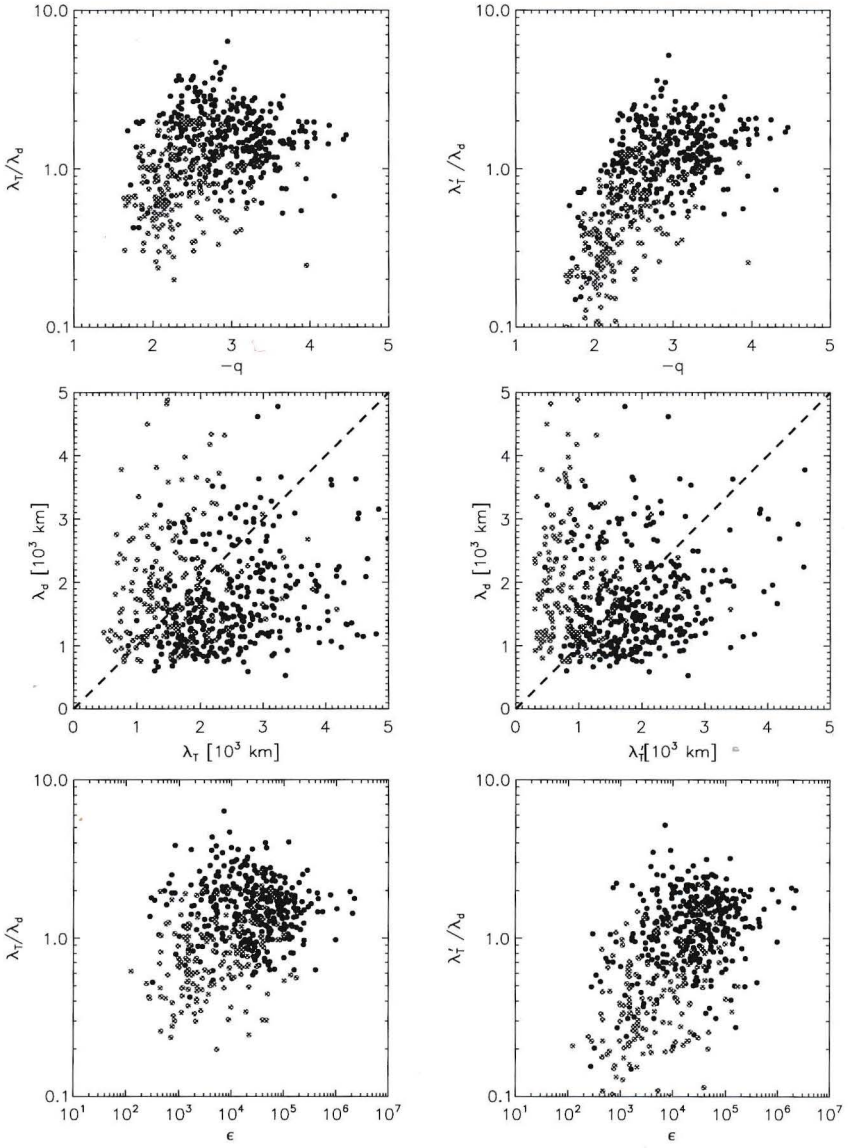

Figure 7. The left column shows the plots before applying the correction ratio to the Taylor microscale λ_T, and the right column shows the Taylor microscale (λ_T') after applying correction ratio.

points appear to be equally scattered. The right column of Figure 7 shows the values of λ_T', after the application of the correction ratio. After the corrections, we can see that the majority of the black points have $\lambda_T' > \lambda_d$ for $q < -3$, and the red points have $\lambda_T' < \lambda_d$ for $q > -3$. This indicates a hydrodynamics type of plasma for open magnetic field case and nonhydrodynamics in the magnetic cloud cases. Further discussion of this analysis is found in *Matthaeus et al.* [2008], where it is argued that the difference in the behavior of these cases points to a difference in relative importance of dissipative processes at ion and electron scales.

4. Conclusions

We have demonstrated a refined technique of calculating the Taylor microscale from a discrete times series by computing correlation functions from structure functions. The method that we employed is based on the definition of the Taylor microscale. To verify this technique we analyze a synthetic time series derived from a defined power density spectrum. We are able to reproduce the Taylor scale values with our technique after applying a correction term, which improves our estimate of the Taylor microscale, estimated from a Richardson extrapolation technique [see *Weygand et al.*, 2009]. In addition, we studied the effects of the dissipation range spectral index and the time resolution of the simulated data. Moreover, we show an example of the

application of the technique to solar wind magnetic field data [*Matthaeus et al.*, 2005, 2008]. This technique is expected to be useful for extracting refined estimates of the Taylor microscale from experimental and observational turbulence data in solar wind and other astrophysical contexts.

Acknowledgments

P. Chuychai was supported by Thailand Research Fund and Thailand's Commission on Higher Education, Ministry of Education (MRG 5286239). J.M. Weygand was partially supported by NSF SHINE: NSF AGS-1155841 and NASA Heliophysics Guest Investigator program NNX09AG31G. W.H. Matthaeus was partially supported by NSF SHINE AGS-1156094 and NASA under the Heliopsheric GI program NNX09AG31G and the Solar Probe Plus project and the Magnetosphere Multiscale project. C.W. Smith is supported by the Advanced Composition Explorer mission. S.D. acknowledges partial support by the Argentinean grant UBACyT 20020120100220 (UBA).

Philippa Browning thanks D. Roberts and an anonymous reviewer for their assistance in evaluating this paper.

References

Alexandrova, O., J. Saur, C. Lacombe, A. Mangeney, J. Mitchell, S. J. Schwartz, and P. Robert (2009), Universality of solar-wind turbulent spectrum from MHD to electron scales, *Phys. Rev. Lett.*, *103*, 165,003.

Batchelor, G. K. (1970), *Theory of Homogeneous Turbulence*, Cambridge Univ. Press, Cambridge, U. K.

Dahlquist, G., and A. Bjorck (2003), *Numerical Methods*, Courier Dover Publications, Mineola, New York, Prentice-Hall 1974.

Dasso, S., W. H. Matthaeus, J. M. Weygand, P. Chuychai, L. J. Milano, C. W. Smith, and M. G. Kivelson (2008), ACE/Wind multispacecraft analysis of the magnetic correlation in the solar wind, in *Proceedings of the 30th International Cosmic Ray Conference. July 3–11, 2007, Mérida, Yucatán, Mexico*, vol. 1, edited by R. Caballero et al., pp. 625–628, Universidad Nacional Autónoma de México, Mexico City, Mexico.

Gary, S. P., and J. E. Borovsky (2004), Alfvén-cyclotron fluctuations: Linear Vlasov theory, *J. Geophys. Res.*, *109*, 6105, doi:10.1029/2004JA010399.

Gurgiolo, C., M. L. Goldstein, W. H. Matthaeus, A. Vinas, and A. N. Fazakerley (2013), Characteristics of the Taylor microscale in the solar wind/foreshock: Magnetic field and electron velocity measurements, *Ann. Geophys.*, *31*, 2063, doi:10.5194/angeo-31-2063-2013.

Hamilton, K., C. W. Smith, B. J. Vasquez, and R. J. Leamon (2008), Anisotropies and helicities in the solar wind inertial and dissipation ranges at 1 AU, *J. Geophys. Res.*, *113*, A01106, doi:10.1029/2007JA012559.

Hinze, J. O. (1975), *Turbulence*, McGraw-Hill, New York.

Leamon, R. J., W. H. Matthaeus, and C. W. Smith (1998), Contribution of cyclotron-resonant damping to kinetic dissipation of interplanetary turbulence, *Astrophys. J.*, *507*, L181, doi:10.1086/311698.

Matthaeus, W. H., and M. L. Goldstein (1982), Stationarity of magnetohydrodynamic fluctuations in the solar wind, *J. Geophys. Res.*, *87*, 10,347–10,354.

Matthaeus, W. H., S. Dasso, J. M. Weygand, L. J. Milano, C. W. Smith, and M. G. Kivelson (2005), Spatial correlation of solar-wind turbulence from two-point measurements, *Phys. Rev. Lett.*, *95*, 231,101, doi:10.1103/PhysRevLett.95.231101.

Matthaeus, W. H., J. M. Weygand, P. Chuychai, S. Dasso, C. W. Smith, and M. Kivelson (2008), Interplanetary magnetic Taylor microscale and implications for plasma dissipation, *Astrophys. J.*, *678*, L141, doi:10.1086/588525.

Sahraoui, F., M. L. Goldstein, P. Robert, and Y. V. Khotyaintsev (2009), Evidence of a cascade and dissipation of solar-wind turbulence at the electron gyroscale, *Phys. Rev. Lett.*, *102*, 231,102, doi:10.1103/PhysRevLett.102.231102.

Smith, C. W., K. Hamilton, J. Vasquez, and R. J. Leamon (2006a), Dependence of the dissipation range spectrum of interplanetary magnetic fluctuations on the rate of energy cascade, *Astrophys. J.*, *645*, L85, doi:10.1086/506151.

Smith, C. W., B. J. Vasquez, and K. Hamilton (2006b), Interplanetary magnetic fluctuation anisotropy in the inertial range, *J. Geophys. Res.*, *111*, A09111, doi:10.1029/2006JA011651.

Taylor, G. I. (1938), The spectrum of turbulence, *Proc. R. Soc. London, Ser. A*, *164*, 476–490.

Weygand, J. M., W. H. Matthaeus, S. Dasso, M. G. Kivelson, and R. J. Walker (2007), Taylor scale and effective magnetic Reynolds number determination from plasma sheet and solar wind magnetic field fluctuations, *J. Geophys. Res.*, *112*, A10201, doi:10.1029/2007JA012486.

Weygand, J. M., W. H. Matthaeus, S. Dasso, M. G. Kivelson, L. M. Kristler, and C. Mouikis (2009), Anisotropy of the Taylor scale and the correlation scale in plasma sheet and solar wind magnetic field fluctuations, *J. Geophys. Res.*, *114*, A07213, doi:10.1029/2008JA013766.

Weygand, J. M., W. H. Matthaeus, M. El-Alaoui, S. Dasso, and M. G. Kivelson (2010), Anisotropy of the Taylor scale and the correlation scale in plasma sheet magnetic field fluctuations as a function of auroral electrojet activity, *J. Geophys. Res.*, *115*, A12250, doi:10.1029/2010JA015499.

Weygand, J. M., W. H. Matthaeus, S. Dasso, and M. G. Kivelson (2011), Correlation and Taylor scale variability in the interplanetary magnetic field fluctuations as a function of solar wind speed, *J. Geophys. Res.*, *116*, A08102, doi:10.1029/2011JA016621.

เอกสารแนบหมายเลข 2

The Astrophysical Journal Letters, 747:L34 (5pp), 2012 March 10 doi:10.1088/2041-8205/747/2/L34

RANDOM BALLISTIC INTERPRETATION OF NONLINEAR GUIDING CENTER THEORY

D. Ruffolo[1,2], T. Pianpanit[1], W. H. Matthaeus[3], and P. Chuychai[2,4]
[1] Department of Physics, Faculty of Science, Mahidol University, Bangkok 10400, Thailand; scdjr@mahidol.ac.th, th_ee@hotmail.com
[2] Thailand Center of Excellence in Physics, CHE, Ministry of Education, Bangkok 10400, Thailand
[3] Bartol Research Institute and Department of Physics and Astronomy, University of Delaware, Newark, DE 19716, USA; yswhm@bartol.udel.edu
[4] School of Science, Mae Fah Luang University, Chiang Rai 57100, Thailand; p.chuychai@sci.mfu.ac.th
Received 2012 January 12; accepted 2012 February 8; published 2012 February 22

ABSTRACT

Nonlinear guiding center (NLGC) theory has been used to explain the asymptotic perpendicular diffusion coefficient $\kappa_\perp$ of energetic charged particles in a turbulent magnetic field, which can be applied to better understand cosmic ray transport. Here we re-derive NLGC, replacing the assumption of diffusive decorrelation with random ballistic decorrelation (RBD), which yields an explicit formula for $\kappa_\perp$. We note that scattering processes can cause a reversal of the guiding center motion along the field line, i.e., "backtracking," leading to partial cancellation of contributions to $\kappa_\perp$, especially for low-wavenumber components of the magnetic turbulence. We therefore include a heuristic backtracking correction (BC) that can be used in combination with RBD. In comparison with computer simulation results for various cases, NLGC with RBD and BC provides a substantially improved characterization of the perpendicular diffusion coefficient for a fluctuation amplitude less than or equal to the large-scale magnetic field.

Key words: diffusion – magnetic fields – turbulence

1. INTRODUCTION

While charged particles subject to a magnetic field in a tenuous plasma will mainly gyrate along that field, magnetic turbulence can cause particles to also spread in the directions perpendicular to the large-scale field. Such perpendicular transport involves an interesting interplay between the transport along field lines, the random walk of magnetic field lines perpendicular to the large-scale field direction, and true cross-field transport in which the particle guiding center eventually separates from its original field line.

The classic FLRW theory (Jokipii 1966), in which particles follow magnetic field lines with a fixed pitch angle, directly related the perpendicular diffusion coefficient $\kappa_\perp$ to the field line diffusion coefficient D. Meanwhile another viewpoint in terms of scattering led to a relation between $\kappa_\perp$ and the parallel diffusion coefficient $\kappa_\parallel$ (Axford 1965; Gleeson 1969). Nonlinear guiding center (NLGC) theory (Matthaeus et al. 2003) successfully accounted for both factors, allowing the guiding center motion to decorrelate due to both parallel (pitch-angle) scattering and the random walk of the guiding magnetic field line, for transverse magnetic fluctuations with a general power spectrum. This theory has provided a much closer match to observations (Bieber et al. 2004) and computer simulation results for $\kappa_\perp$ (see also Minnie et al. 2007; Ruffolo et al. 2008), and its framework has attracted theoretical interest and inspired numerous related theories (e.g., Shalchi et al. 2004, 2006; le Roux & Webb 2007; Qin 2007; Shalchi 2010).

The original NLGC theory (Matthaeus et al. 2003) used the Taylor–Green–Kubo (TGK) formula (Taylor 1922; Green 1951; Kubo 1957)

$$\kappa_{xx} \equiv \lim_{t\to\infty} \frac{\langle \Delta x^2 \rangle}{2t} = \int_0^\infty \langle \tilde{v}_x(0)\tilde{v}_x(t)\rangle dt \qquad (1)$$

for the asymptotic particle diffusion coefficient κ_{xx} along a coordinate x perpendicular to the large-scale magnetic field direction z, based on the guiding center velocity $\tilde{\mathbf{v}}$. That work used

$$\langle \tilde{v}_x(0)\tilde{v}_x(t)\rangle \approx \frac{a^2}{B_0^2}\langle v_z(0)v_z(t)\rangle\langle b_x(0,0)b_x[\mathbf{x}(t),t]\rangle, \qquad (2)$$

for the displacement $\mathbf{x}(t)$ of the particle guiding center trajectory in a large-scale magnetic field $B_0\hat{\mathbf{z}}$. The authors set $a^2 = 1/3$, a factor which effectively accounts for the replacement of $\tilde{v}_z$ with the particle velocity v_z in the correlations. Then the Lagrangian correlation $\langle b_x(0,0)b_x[\mathbf{x}(t),t]\rangle$ was evaluated in terms of the Eulerian correlation function and power spectrum by using Corrsin's independence hypothesis (Corrsin 1959) and setting the displacement distribution to that for asymptotic diffusion (Salu & Montgomery 1977), leading to an implicit formula for $\kappa_\perp$ in terms of input values of κ_{zz} and the power spectrum of magnetic fluctuations. A related approach was previously used to derive a field line diffusion coefficient (Matthaeus et al. 1995) that is reasonably close to values from direct computer simulations (Gray et al. 1996; Ghilea et al. 2011).

In the present work, we consider an alternate interpretation of NLGC that replaces the diffusive distribution of guiding center trajectories with a random ballistic distribution, for the purpose of calculating the Lagrangian magnetic correlation function $\langle b_x(0,0)b_x[\mathbf{x}(t),t]\rangle$. This approach was recently introduced for calculating the field line diffusion coefficient and led to some substantial improvements in the match with direct simulation results (Ghilea et al. 2011). It is analogous to concepts in random walk theory in which the mean free path is determined by the extent of ballistic motion between scattering events. In this context, note that $\tilde{v}_x$ decorrelates over the decorrelation scale of v_z or b_x, whichever is shorter. This implies that the decorrelation of $\tilde{v}_x$ in the TGK integral (which determines κ_{xx}) takes place over a distance scale for which the parallel motion is approximately constant and the field lines are approximately straight, so the guiding center motion can be treated as ballistic in random directions determined by the distribution of magnetic field directions (Figure 1). (As illustrated in the figure, at longer times the guiding center velocity will change, the particle will reverse its direction along $\mathbf{B}$, and the particle will depart from its original guiding field line.) We demonstrate that this

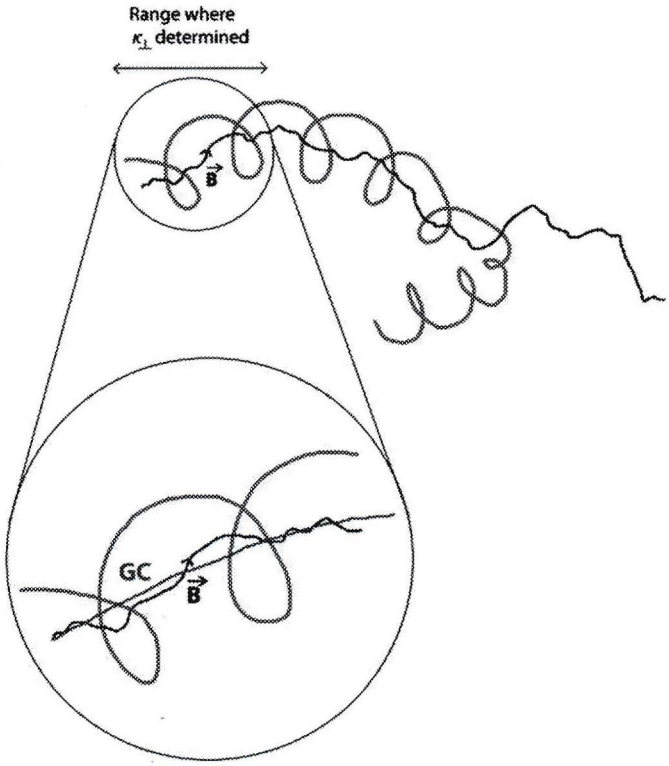

Figure 1. Illustration of the random ballistic interpretation of nonlinear guiding center (NLGC) theory. The diffusion coefficient $\kappa_\perp$ of energetic charged particle motion (red line) perpendicular to the large-scale magnetic field is related to the decorrelation (i.e., change in direction) of a perpendicular component of the guiding center velocity (GC, blue line), which roughly follows a local magnetic field line (black line). Over the relevant distance scale, the guiding center motion can be approximated as ballistic (i.e., with constant velocity) along random directions distributed like the magnetic field directions. Such random ballistic decorrelation (RBD) is determined using the framework of NLGC theory, including the effects of the field line random walk and the parallel scattering of particle trajectories.

approach, together with a backtracking correction (BC), leads to a substantial improvement in the match with direct computer simulations of the perpendicular diffusion of energetic charged particles.

2. RANDOM BALLISTIC DECORRELATION

We consider the application of Corrsin's independence hypothesis (described below) assuming a Gaussian distribution of displacements, where diffusive decorrelation (DD) or random ballistic decorrelation (RBD) is used to describe the variance σ_i^2 along each direction. DD considers that the asymptotic diffusion also governs the displacement distribution at early times during the decorrelation process, so $\sigma_i^2 = 2\kappa_{ii}t$, while RBD assumes the decorrelation is determined by ballistic motion of guiding centers at early times in random directions, at guiding center velocity $\tilde{\mathbf{v}}$, depending on the fluctuating magnetic field, with $\sigma_i^2 = \langle\tilde{v}_i^2\rangle t^2$.

Let us assume axisymmetry, define the fluctuation amplitude b so that $b^2 = \langle b_x^2 + b_y^2\rangle = 2\langle b_x^2\rangle$, and define v_s as the particle velocity along the local magnetic field. As a special case of Equation (2) for $t = 0$, we use

$$\langle\tilde{v}_x^2\rangle = \langle\tilde{v}_y^2\rangle \approx \frac{a^2}{B_0^2}\langle v_z^2\rangle\langle b_x^2\rangle = \frac{a^2v^2}{6}\frac{b^2}{B_0^2}, \tag{3}$$

where we use $\langle v_z^2\rangle = v^2/3$ for an isotropic distribution of particle velocities. We also use $\langle\tilde{v}^2\rangle = v^2/3$ to obtain

$$\langle\tilde{v}_z^2\rangle = \frac{v^2}{3}\left(1 - a^2\frac{b^2}{B_0^2}\right). \tag{4}$$

Note that for $b/B_0 > a^{-1} = \sqrt{3}$, Equation (4) gives a nonsensical negative value for $\langle\tilde{v}_z^2\rangle$. Thus, we will consider this RBD approach to be limited to $b/B_0 \leqslant \sqrt{3}$. Note that the NLGC framework in general is also limited to magnetic fluctuation amplitudes that are not too great, in the sense that NLGC assumes transverse fluctuations, and if $b \gg B_0$ one would not expect the (weak) mean magnetic field to force the fluctuations to be strongly transverse.

As in the original derivation of NLGC, we use Equations (1) and (2), with $\langle v_z(0)v_z(t)\rangle = (v^2/3)e^{-t/\tau}$ for a pitch-angle scattering time τ, to obtain

$$\kappa_{xx} = \frac{a^2v^2}{3B_0^2}\int_0^\infty e^{-t/\tau}\langle b_x(0,0)b_x[\mathbf{x}(t),t]\rangle dt. \tag{5}$$

We then make use of Corrsin's independence hypothesis to relate the Lagrangian correlation $\langle b_x(0,0)b_x[\mathbf{x}(t),t]\rangle$ to the Eulerian correlation function R_{xx} and the probability of displacement $\mathbf{x}$ at time t, so that

$$\kappa_{xx} = \frac{a^2v^2}{3B_0^2}\int_0^\infty e^{-t/\tau}\int R_{xx}(\mathbf{x},t)P(\mathbf{x}|t)d\mathbf{x}\,dt. \tag{6}$$

Following Matthaeus et al. (2003), we use the Fourier transform of the correlation function $R_{xx}(\mathbf{x},t)$ as the power spectrum $S_{xx}(\mathbf{k},t) = S_{xx}(\mathbf{k})e^{-\gamma(\mathbf{k})t}$ and assume independent guiding center displacement probability distributions along each coordinate to obtain

$$\kappa_{xx} = \frac{a^2v^2}{3B_0^2}\int_0^\infty e^{-t/\tau}\int S_{xx}(\mathbf{k})e^{-\gamma(\mathbf{k})t}\left(\int_{-\infty}^\infty e^{-ik_xx}P(x|t)dx\right) \times\left(\int_{-\infty}^\infty e^{-ik_yy}P(y|t)dy\right)\left(\int_{-\infty}^\infty e^{-ik_zz}P(z|t)dz\right)d\mathbf{k}\,dt. \tag{7}$$

For a Gaussian displacement distribution $P(x|t)$, we have (Ghilea et al. 2011)

$$\int_{-\infty}^\infty e^{-ik_xx}P(x|t)dx = \exp\left(-\frac{1}{2}k_x^2\sigma_x^2\right) \tag{8}$$

and analogous formulas for y and z. For RBD we use $\sigma_i^2 = \langle\tilde{v}_i^2\rangle t^2$, and substituting Equation (8) into Equation (7) yields

$$\kappa_{xx} = \frac{a^2v^2}{3B_0^2}\int S_{xx}(\mathbf{k})T(\mathbf{k})\,d\mathbf{k}, \tag{9}$$

where the mean free time $T(\mathbf{k})$ is given by

$$T(\mathbf{k}) = \int_0^\infty \exp\left[-\frac{t}{\tau} - \gamma(\mathbf{k})t - \frac{1}{2}\sum_i k_i^2\langle\tilde{v}_i^2\rangle t^2\right]dt. \tag{10}$$

Performing the t-integration and using $1/\tau = v/\lambda_\parallel = v^2/(3\kappa_{zz})$, we obtain

$$T(\mathbf{k}) = \sqrt{\frac{\pi}{2}}\frac{e^{\alpha^2}\,\mathrm{erfc}(\alpha)}{\sqrt{\sum_i k_i^2\langle\tilde{v}_i^2\rangle}} \tag{11}$$

and

$$\kappa_{xx} = \frac{a^2 v^2}{3B_0^2}\sqrt{\frac{\pi}{2}}\int \frac{S_{xx}(\mathbf{k})}{\sqrt{\sum_i k_i^2\langle\tilde{v}_i^2\rangle}}\, e^{\alpha^2}\,\mathrm{erfc}(\alpha)d\mathbf{k} \qquad \text{(RBD)}, \tag{12}$$

where

$$\alpha \equiv \frac{v^2/(3\kappa_{zz}) + \gamma(\mathbf{k})}{\sqrt{2\sum_i k_i^2\langle\tilde{v}_i^2\rangle}} \tag{13}$$

and the expressions for $\langle\tilde{v}_i^2\rangle$ are given by Equations (3) and (4).

Note that the original DD interpretation of Matthaeus et al. (2003) used the formula for asymptotic diffusion with κ_{xx} in the displacement distribution, yielding an implicit equation for κ_{xx}. In contrast, the RBD theory uses a predetermined random ballistic formula for the displacement distribution and yields an explicit formula for κ_{xx}, as in analogous theories for the field line diffusion coefficient (Ghilea et al. 2011). For numerical evaluation, NLGC-type theories based on DD typically require an iterative solution, whereas NLGC/RBD can be evaluated without iteration.

3. BACKTRACKING CORRECTION

Previous simulations have shown that the perpendicular transport of energetic charged particles is characterized by ballistic (free-streaming) guiding center motion at short times, followed by subdiffusion (Qin et al. 2002a) and later, if the fluctuations have sufficient transverse complexity, by asymptotic diffusion (Qin et al. 2002b). This subdiffusion is due to a parallel (pitch-angle) scattering process that causes a particle to reverse its motion along the local field line and partially retrace its steps. Such "backtracking" leads to a negative v_x-correlation function over a certain time range, hence the reduction in the running perpendicular diffusion coefficient. In some cases this leads to subdiffusion (see Qin et al. 2002b and Section 4 of Ruffolo et al. 2008).

Backtracking was inherent in the original NLGC/DD theory (Matthaeus et al. 2003). The use of diffusive displacements means that the displacements for which the correlation function is sampled can undergo a random walk, including backtracking. It was assumed that backtracking did not completely cancel out the perpendicular guiding center excursions due to other physical effects. This is not the case for the RBD calculation, which is based on ballistic guiding center trajectories.

For RBD theory, we note that Equations (9) and (10) assign a mean free time $T(\mathbf{k})$ to individual $\mathbf{k}$-components of the turbulence, which are averaged with weighting according to the power spectrum, to determine κ_{xx}. Conceptually this relates to the v_z–b_x independence hypothesis of Matthaeus et al. (2003). For magnetostatic fluctuations with $\gamma = 0$, Equation (11) gives $T \approx \tau$ for low k and T decreases for higher k. Thus, for modes of low k, the mean free time is determined by the parallel scattering, whereas for higher k it is determined by the field line random walk.

This random ballistic calculation of the mean free time does not account for backtracking. Consider low k, for which the decorrelation in Equation (10) is dominated by the scattering term (first term in the exponential) while $\mathbf{b}$ is nearly constant. Then the perpendicular displacement associated with $T(\mathbf{k})$ will be largely canceled out by subsequent backtracking. A similar effect leads to subdiffusion in simulation results (i.e., running κ_{xx} decreases with increasing t) for fluctuations with insufficient transverse complexity (Qin et al. 2002a), whereas NLGC yields a much larger asymptotic value of κ_{xx} (see Run 12 of Ruffolo et al. 2008).

Therefore, we introduce a heuristic BC for RBD that reduces the influence of such low-k modes by reducing $T(\mathbf{k})$ and therefore their contribution to the overall κ_{xx}. We multiply $T(\mathbf{k})$ by $e^{-\alpha^2}$, which simplifies Equation (11) to yield

$$T(\mathbf{k}) = \sqrt{\frac{\pi}{2}}\frac{\mathrm{erfc}(\alpha)}{\sqrt{\sum_i k_i^2\langle\tilde{v}_i^2\rangle}} \tag{14}$$

and

$$\kappa_{xx} = \frac{a^2 v^2}{3B_0^2}\sqrt{\frac{\pi}{2}}\int \frac{S_{xx}(\mathbf{k})}{\sqrt{\sum_i k_i^2\langle\tilde{v}_i^2\rangle}} \times \mathrm{erfc}\left[\frac{v^2/(3\kappa_{zz}) + \gamma(\mathbf{k})}{\sqrt{2\sum_i k_i^2\langle\tilde{v}_i^2\rangle}}\right] d\mathbf{k} \quad \text{(RBD/BC)}. \tag{15}$$

This BC is related to the terms that are linear and quadratic in t, in the exponential of Equation (10). Here, $e^{-\alpha^2}$ serves as a simple "switch" that is close to 0 when k is sufficiently low that the linear term dominates, suggesting a strong effect of backtracking, while it approaches 1 for higher k. Note also that for a given $\mathbf{k}$, there is a time t when the linear and quadratic terms are equal, i.e., the field line random walk becomes important. At that time we have $t/\tau \sim \alpha^2$, and substitution into the parallel velocity correlation term $e^{-t/\tau}$ suggests the use of $e^{-\alpha^2}$ to account for backtracking effects.

4. NUMERICAL EVALUATION OF ANALYTIC THEORIES USING 2D+slab TURBULENCE

To numerically evaluate analytic theories for comparison with computer simulation results, we need to specify the power spectrum. We employ a two-component 2D+slab model of transverse magnetic fluctuations in which the power spectrum is a sum of a two-dimensional (2D) power spectrum, depending on k_x and k_y, and a slab power spectrum depending on k_z. The latter represents parallel Alfvénic fluctuations and the former idealizes the quasi-2D structures, including "flux tubes," that can develop from interactions of such waves (Shebalin et al. 1983; see also Borovsky 2008; Seripienlert et al. 2010; and references therein). The two-component model was motivated by observations of interplanetary magnetic fluctuations, indicating quasi-slab and quasi-2D components (Matthaeus et al. 1990; Weygand et al. 2009), which can be modeled using a ratio of slab:2D fluctuation energies of approximately 20:80 (Bieber et al. 1994, 1996). This model has provided a useful description of the parallel transport of particles in the inner heliosphere (Bieber et al. 1994), and was used by most studies that implemented and/or tested NLGC theory.

For the special case of 2D+slab fluctuations, Equations (12) and (15) and their DD equivalent split into two terms using S_{xx}^{slab} and S_{xx}^{2D}. However, Shalchi (2006) has proposed that the direct contribution of slab fluctuations to the perpendicular transport should be subdiffusive, and that the S_{xx}^{slab} term should not be included in the equation of $\kappa_\perp$. (Note that slab fluctuations can still play a role as a key determinant of $\lambda_\parallel$, which enters into the 2D contribution.) We refer to this proposal as the Shalchi slab hypothesis. We employ this in the present work, and a detailed evaluation of its accuracy will be presented in a future publication (D. Ruffolo et al., in preparation).

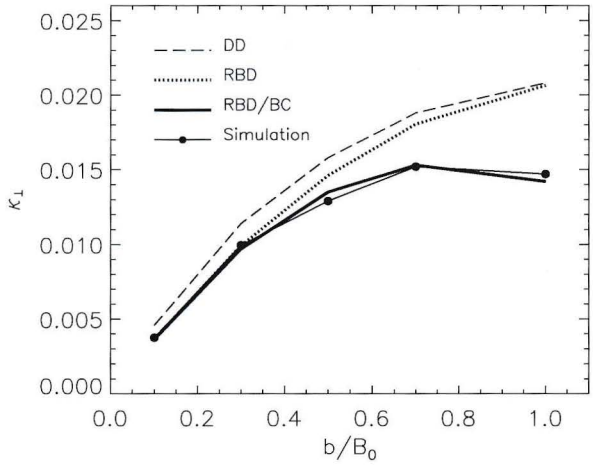

Figure 2. Asymptotic perpendicular diffusion coefficient $\kappa_\perp$ of 100 MeV protons in 2D+slab turbulence with a slab fraction $f_s = 0.2$ as a function of the magnetic fluctuation amplitude b/B_0. Using the NLGC framework, random ballistic decorrelation with backtracking correction (RBD/BC, thick line) provides a closer match with computer simulation results (solid circles) than the original DD theory (long-dashed line) and uncorrected RBD (short-dashed line). In the present work we also employ the Shalchi slab hypothesis (Shalchi 2006).

Therefore, when using the 2D+slab model of magnetic turbulence, in Equation (12) or Equation (15) we include only the 2D portion of the power spectrum, which is concentrated at $k_z = 0$. We also assume the fluctuations to be magnetostatic, with $\gamma = 0$, and axisymmetric. For RBD without the BC, we have

$$\kappa_{xx} = \frac{a^2 v^2}{3B_0^2}\sqrt{\frac{\pi}{2}}\int_{-\infty}^{\infty}\int_{-\infty}^{\infty} \times \frac{S_{xx}^{2D}(k_x,k_y)}{k_\perp\sqrt{\langle\tilde{v}_x^2\rangle}}\, e^{\alpha^2}\,\mathrm{erfc}(\alpha)dk_x dk_y \qquad \text{(RBD)}, \quad (16)$$

and with the BC we have

$$\kappa_{xx} = \frac{a^2 v^2}{3B_0^2}\sqrt{\frac{\pi}{2}}\int_{-\infty}^{\infty}\int_{-\infty}^{\infty} \times \frac{S_{xx}^{2D}(k_x,k_y)}{k_\perp\sqrt{\langle\tilde{v}_x^2\rangle}}\,\mathrm{erfc}(\alpha)dk_x dk_y \qquad \text{(RBD/BC)}, \quad (17)$$

where

$$\alpha = \frac{v^2}{3\kappa_{zz}k_\perp\sqrt{2\langle\tilde{v}_x^2\rangle}} \quad (18)$$

and $k_\perp^2 = k_x^2 + k_y^2$.

For comparison, we also consider the original DD theory, and for our model assumptions we obtain

$$\kappa_{xx} = \frac{a^2 v^2}{3B_0^2}\int_{-\infty}^{\infty}\int_{-\infty}^{\infty}\frac{S_{xx}^{2D}(k_x,k_y)dk_x dk_y}{v^2/(3\kappa_{zz}) + k_\perp^2\kappa_{xx}} \qquad \text{(DD)}. \quad (19)$$

The analytic theory expressions were evaluated numerically using the MATHEMATICA program (Wolfram Research, Inc.) to perform continuous **k**-space integrals. For the input value of κ_{zz}, we used the simulation value.

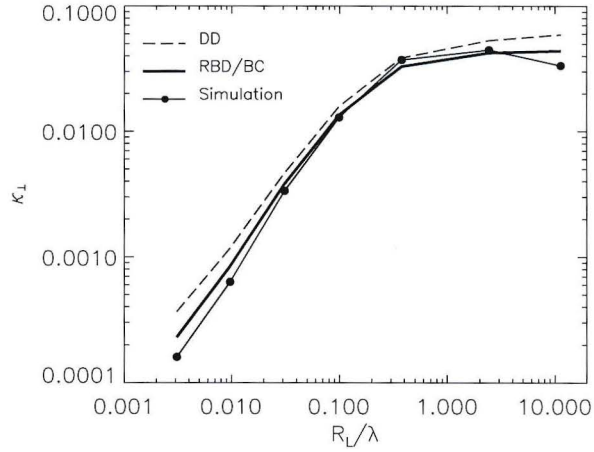

Figure 3. Asymptotic perpendicular diffusion coefficient $\kappa_\perp$ in 2D+slab turbulence with $f_s = 0.2$ and $b/B_0 = 0.5$ as a function of the proton gyroradius in units of the turbulence bendover scale. The simulation values shown here (solid circles) correspond to proton energies ranging from 0.1 MeV to 50 GeV for $B_0 = 5$ nT and $\lambda = 0.02$ AU. In most cases, the RBD/BC theory (thick line) provides a better explanation of the computer simulation results (solid circles) than the original DD theory (dashed line).

5. COMPARISON WITH COMPUTER SIMULATIONS

We have also performed direct computer simulations to trace particle orbits in 2D+slab magnetic turbulence. While the simulations inevitably involve some discretization and statistical errors, they do avoid key assumptions of the analytic work, and thus provide an independent check of their validity.

The computer simulations were performed using the methods, power spectra, and parameter values described by Ruffolo et al. (2008). In particular, all distances are in units of $\lambda = 0.02$ AU, the slab and 2D turbulence bendover scale,[5] and velocities are in units of the speed of light c. Simulations were performed over a sufficient time for all κ_{ii} to approach asymptotic values, within statistical errors. We assume axisymmetry about the large-scale field direction, so κ_{xx} and κ_{yy} should be the same within statistical errors, which we verified in all cases. We report $\kappa_\perp \equiv (\kappa_{xx} + \kappa_{yy})/2$, which can be compared directly with κ_{xx} from theories. In some contexts, we use $\kappa_\perp$ as a synonym for κ_{xx}.

Figure 2 shows the dependence of $\kappa_\perp$ (in units of $c\lambda$) on the overall fluctuation amplitude b/B_0, using $f_s \equiv b_{\rm slab}^2/(b_{\rm slab}^2 + b_{\rm 2D}^2) = 0.2$. It is apparent that the RBD/BC version (thick lines) agrees with computer simulation results (solid circles) better and over a wider range of b/B_0 values than either the DD theory (long-dashed lines) or RBD without the BC (short-dashed lines), over the range of applicability of RBD ($b/B_0 \leqslant 1/a = \sqrt{3}$). We have also examined the dependence on the proton gyroradius (Figure 3), which is related to its energy, for fixed $f_s = 0.2$ and $b/B_0 = 0.5$. The seven simulations were for protons of kinetic energy 0.1, 1, 10, and 100 MeV as well as 1, 10, and 50 GeV. The RBD results, not shown, nearly match DD at $R_L/\lambda < 1$, nearly match RBD/BC at $R_L/\lambda > 1$, and are intermediate at $R_L/\lambda \approx 1$. Overall, the RBD/BC theory again provides the best explanation of the computer simulation results.

[5] Ruffolo et al. (2008) incorrectly specified $\lambda = 0.027$ AU; their simulations actually used $\lambda = 0.02$ AU, and calculations were performed for the same parameters as the simulations.

6. DISCUSSION

In the present work, we interpret NLGC theory in terms of particle guiding center trajectories that are ballistic with constant velocity over the distance scale leading up to their decorrelation (Figure 1), a standard assumption in random walk theory based on scattering concepts. Such RBD stands in contrast to the previous assumption of DD in which the displacements were taken to spread according to asymptotic diffusion. The use of Corrsin's hypothesis for RBD is similar in spirit to a Fokker–Planck approach in which the unperturbed trajectory has a constant but random velocity whose directional distribution is related to the distribution of magnetic fluctuations. It is also related to the Langevin-equation approaches of Balescu et al. (1994). Our use of a heuristic BC that is specific to RBD leads to a substantial improvement in the match with direct computer simulation results, compared with DD and RBD without BC.

Note that RBD theory does not require a small fluctuation amplitude, and indeed RBD/BC matches computer simulation results very well for amplitudes up to $b/B_0 \sim 1$ (Figure 2). The inapplicability for $b/B_0 > 1/a = \sqrt{3}$ indicates room for future improvements to obtain a truly non-perturbative theory. At the same time, we should note that the NLGC framework treats only transverse magnetic fluctuations. In the interplanetary medium of the inner heliosphere, transverse fluctuations account for ~90% of the magnetic fluctuation energy (Belcher & Davis 1971), so NLGC is well justified in this case. However, for large amplitudes with $b/B_0 \gg 1$ there is little reason for the fluctuations to be so strongly anisotropic, and the NLGC framework itself may have limited applicability.

Considering the dependence of $\kappa_\perp$ on the proton Larmor radius, R_L, as shown in Figure 3, a discrepancy remains between NLGC theory and simulation results for the two lowest energies, 0.1 and 1 MeV. The discrepancy is substantially reduced for RBD/BC. For energies of 10 MeV to 10 GeV (i.e., $R_L/\lambda = 0.031$–2.4), RBD/BC theory matches the simulation results very well. The increase with R_L/λ saturates in this range because $\kappa_\perp$ is roughly proportional to v (Minnie et al. 2009), which saturates at c.

The NLGC framework in general could break down when $R_L/\lambda \gg 1$. In this weak scattering limit NLGC considers that guiding center motion tracks the local field line random walk, whereas such a large gyroradius implies that particles experience fluctuations independent from those at the guiding center, and low-wavelength fluctuations should have less influence on perpendicular diffusion when they are averaged over such a large gyroradius. In the interplanetary magnetic field near Earth of about 5 nT with $\lambda \sim 0.02$ AU (Jokipii & Coleman 1968), we have $R_L \sim \lambda$ for a proton energy of about 4 GeV, and in the local galactic magnetic field of about 0.4 nT (Opher et al. 2009), where $\lambda \sim 100$ pc (Armstrong et al. 1995; Dyson & Williams 1997), we have $R_L \sim \lambda$ for a proton energy of $\sim 4 \times 10^{17}$ eV.

We have searched for and found this effect at the highest proton energy considered, 50 GeV, which corresponds to $R_L/\lambda = 11$ for our parameter values of $B_0 = 5$ nT, $b/B_0 = 0.5$, and $f_s = 0.2$, which are applicable to the interplanetary medium near Earth. The perpendicular diffusion coefficient $\kappa_\perp$ decreases, presumably due to cancellation of low-wavelength fluctuations over the gyro-orbit, while all NLGC theories predict a slight increase. In any case, the above energies where $R_L \sim \lambda$ for interplanetary and interstellar propagation are sufficiently high that NLGC theories remain applicable to a wide range of cosmic ray and energetic particle transport problems.

This work was partially supported by the Development and Promotion of Science and Technology Talents Project of the Royal Thai Government, the U.S. NSF (AGS-1063439 and SHINE AGS-1156094), NASA (Heliophysics Theory NNX11AJ4G), the Solar Probe Plus/ISIS project, and the Thailand Research Fund and Thailand's Commission on Higher Education, Ministry of Education (MRG 5286239). We thank Achara Seripienlert for technical assistance.

REFERENCES

Armstrong, J. W., Rickett, B. J., & Spangler, S. R. 1995, ApJ, 443, 209
Axford, W. I. 1965, Planet. Space Sci., 13, 115
Balescu, R., Wang, H.-D., & Misguich, J. H. 1994, Phys. Plasmas, 1, 3826
Belcher, J. W., & Davis, L., Jr. 1971, J. Geophys. Res., 76, 3534
Bieber, J. W., Matthaeus, W. H., Shalchi, A., & Qin, G. 2004, Geophys. Res. Lett., 31, L10805
Bieber, J. W., Matthaeus, W. H., Smith, C. W., et al. 1994, ApJ, 420, 294
Bieber, J. W., Wanner, W., & Matthaeus, W. H. 1996, J. Geophys. Res., 101, 2511
Borovsky, J. E. 2008, J. Geophys. Res., 113, A08110
Corrsin, S. 1959, in Atmospheric Diffusion and Air Pollution, ed. F. Frenkel & P. Sheppard (Advances in Geophysics, Vol. 6; New York: Academic), 161
Dyson, J. E., & Williams, D. A. (ed.) 1997, in The Graduate Series in Astronomy, The Physics of the Interstellar Medium (2nd ed.; Bristol: Institute of Physics Publishing)
Ghilea, M. C., Ruffolo, D., Chuychai, P., et al. 2011, ApJ, 741, 16
Gleeson, L. J. 1969, Planet. Space Sci., 17, 31
Gray, P. C., Pontius, D. H., Jr., & Matthaeus, W. H. 1996, Geophys. Res. Lett., 23, 965
Green, M. S. 1951, J. Chem. Phys., 19, 1036
Jokipii, J. R. 1966, ApJ, 146, 480
Jokipii, J. R., & Coleman, P. J. 1968, J. Geophys. Res., 73, 5495
Kubo, R. 1957, J. Phys. Soc. Japan, 12, 570
le Roux, J. A., & Webb, G. M. 2007, ApJ, 667, 930
Matthaeus, W. H., Goldstein, M. L., & Roberts, D. A. 1990, J. Geophys. Res., 95, 20673
Matthaeus, W. H., Gray, P. C., Pontius, D. H., Jr., & Bieber, J. W. 1995, Phys. Rev. Lett., 75, 2136
Matthaeus, W. H., Qin, G., Bieber, J. W., & Zank, G. 2003, ApJ, 590, L53
Minnie, J., Bieber, J. W., Matthaeus, W. H., & Burger, R. A. 2007, ApJ, 663, 1049
Minnie, J., Matthaeus, W. H., Bieber, J. W., Ruffolo, D., & Burger, R. A. 2009, J. Geophys. Res., 114, A01102
Opher, M., Alouani Bibi, F., Toth, G., et al. 2009, Nature, 462, 1036
Qin, G. 2007, ApJ, 656, 217
Qin, G., Matthaeus, W. H., & Bieber, J. W. 2002a, Geophys. Res. Lett., 29, 7
Qin, G., Matthaeus, W. H., & Bieber, J. W. 2002b, ApJ, 578, L117
Ruffolo, D., Chuychai, P., Wongpan, P., et al. 2008, ApJ, 686, 1231
Salu, Y., & Montgomery, D. C. 1977, Phys. Fluids, 20, 1
Seripienlert, A., Ruffolo, D., Matthaeus, W. H., & Chuychai, P. 2010, ApJ, 711, 980
Shalchi, A. 2006, A&A, 453, L43
Shalchi, A. 2010, ApJ, 720, L127
Shalchi, A., Bieber, J. W., Matthaeus, W. H., & Qin, G. 2004, ApJ, 616, 617
Shalchi, A., Bieber, J. W., Matthaeus, W. H., & Schlickeiser, R. 2006, ApJ, 642, 230
Shebalin, J. V., Matthaeus, W. H., & Montgomery, D. 1983, J. Plasma Phys., 29, 525
Taylor, G. I. 1922, Proc. London Math. Soc. Ser. 2, 20, 196
Weygand, J. M., Matthaeus, W. H., Dasso, S., et al. 2009, J. Geophys. Res., 114, A07213